Boletim da Sociedade Astronômica Brasileira, **37**, no. 1, 329-333

HE and VHE gamma-ray observations of the blazars 3C 279 and PKS 2155-304

Samuel Victor Bernardo da Silva[1], Vinícius Mendonça de Lima Barros[2], & Luiz Augusto Stuani Pereira[2,3]

[1] Departamento de Física, Universidade Federal do Espírito Santo, Núcleo de Astrofísica e Cosmologia (Cosmo-Ufes) e-mail: samuel.vb.silva@edu.ufes.br
[2] Universidade Federal de Campina Grande e-mail: viniciusmendoca526@gmail.com
[3] Universidade de São Paulo e-mail: luizstuani@uaf.ufcg.edu.br

Abstract. 3C 279 is a Flat Spectrum Radio Quasar (FSRQ) at $z = 0.536$, first detected by the Rosemary Hill Observatory (RHO) in 1971. This source exhibited intense activity between 2017 and 2018, characterized by multiple flaring events at high energies. The BL Lac object PKS 2155-304 at $z = 0.116$ was observed by the High Energy Stereoscopic System (H.E.S.S.) in July 2006 during extraordinary outbursts of very-high-energy gamma-ray emission. In this work, we model the spectral energy distributions (SEDs) of these sources assuming a leptonic origin. A single-zone model is adopted, considering a spherical region, referred to as a *blob*, within the relativistic jet. This region contains a non-thermal distribution of electrons and positrons and is permeated by a uniform magnetic field. Leptonic particles within the blob interact with the magnetic field, producing synchrotron radiation that spans from radio frequencies to soft X-rays. These synchrotron photons are subsequently upscattered to higher energies by the same population of electrons via the inverse Compton process, resulting in a high-energy and very-high-energy gamma-ray spectrum. Furthermore, a lepto-hadronic scenario is explored to account for the broadband emission. In this framework, we include the interaction of relativistic protons with the ambient photon field via photomeson production and Bethe-Heitler pair production processes. These interactions initiate electromagnetic cascades and generate secondary decay products that contribute significantly to the high-energy gamma-ray flux and imply potential neutrino emission. This scenario provides a more comprehensive explanation for the high-energy component of the SED.

Resumo. 3C 279 é um Quasar de Rádio de Espectro Plano (FSRQ) em $z = 0,536$, detectado pela primeira vez pelo Observatório Rosemary Hill (RHO) em 1971. Esta fonte exibiu atividade intensa entre 2017 e 2018, caracterizada por múltiplos eventos de flares em altas energias. O objeto BL Lac PKS 2155-304 em $z = 0,116$ foi observado pelo High Energy Stereoscopic System (H.E.S.S.) em julho de 2006 durante surtos extraordinários de emissão de raios gama de energia muito alta. Neste trabalho, modelamos as distribuições espectrais de energia (SEDs) dessas fontes assumindo uma origem leptônica. Adota-se um modelo de zona única, no qual consideramos uma região esférica, denominada *blob*, localizada no interior do jato relativístico. Esta região contém uma distribuição não térmica de elétrons e pósitrons e é permeada por um campo magnético uniforme. As partículas leptônicas dentro do *blob* interagem com o campo magnético, produzindo radiação síncrotron que se estende desde frequências de rádio até raios X moles. Esses fótons síncrotron são subsequentemente espalhados para energias mais altas pela mesma população de elétrons via processo Compton inverso, resultando em um espectro de raios gama de alta e muito alta energia. Além disso, explora-se um cenário lepto-hadrônico para explicar a emissão em banda larga. Neste contexto, incluímos a interação de prótons relativísticos com o campo de fótons ambiente através de processos de produção de fotomésons e de pares de Bethe-Heitler. Essas interações iniciam cascatas eletromagnéticas e geram produtos de decaimento secundários que contribuem significativamente para o fluxo de raios gama de alta energia e implicam a potencial emissão de neutrinos. Este cenário fornece uma explicação mais abrangente para a componente de alta energia da SED.

Keywords. Galaxies: active – Data analysis–Radiation mechanisms: non-thermal

1. Introduction

Blazars, a subclass of Active Galactic Nuclei (AGN) with relativistic jets oriented close to our line of sight, exhibit broadband emission spanning from radio to very-high-energy gamma rays Cerruti et al. (2012a); Gharutyunyan et al. (2025). Based on the strength of their optical emission lines, these sources are primarily classified into BL Lac objects, which display weak or absent lines, and Flat Spectrum Radio Quasars (FSRQs), which exhibit strong broad lines Gharutyunyan et al. (2025).

The broadband emission of these sources is characterized by a double-humped spectral energy distribution (SED). The low-energy hump is typically attributed to synchrotron radiation from relativistic electrons, while the high-energy hump is generally ascribed to the inverse Compton scattering of these photons Krishna Mohana et al. (2025); Weidinger & Spanier (2010). This fundamental understanding forms the basis for investigating the physical mechanisms driving the observed radiation from blazars Krishna Mohana et al. (2025).

However, the exact mechanisms responsible for the high-energy emission, particularly the second hump, remain a subject of ongoing debate Abdalla et al. (2019). While leptonic models attribute this emission to inverse Compton scattering, hadronic scenarios offer a comprehensive alternative, proposing that the second hump is caused by processes initiated by a population of relativistic protons, such as proton synchrotron emission or photo-pion cascades Bharathan et al. (2025); Lucchini et al. (2018); Bernardo da Silva et al. (2025).

2. Blazar Sources Overview

In this work, we investigated two distinct types of blazars. The source 3C 279 is a Flat Spectrum Radio Quasar (FSRQ) located at redshift $z = 0.536$ (Lynds et al. 1965). Historically significant, it was one of the first gamma-ray emitting blazars discovered by the EGRET telescope (Hartman et al. 1992). Furthermore, it holds the distinction of being the first FSRQ detected in the very high

energy (VHE, $E > 100$ GeV) regime by the MAGIC telescopes, making it one of the most distant VHE sources known (Errando et al. 2008). This source exhibits strong variability across the entire electromagnetic spectrum, with a gamma-ray flux that can vary by more than two orders of magnitude. Multi-wavelength monitoring has revealed complex correlation patterns; for instance, gamma-ray emission has been observed to precede optical emission by approximately 10 days, and "orphan" X-ray flares have been recorded. Radio observations using VLBA have revealed superluminal motion with apparent velocities of $\sim 20c$, allowing for the estimation of jet parameters such as the bulk Lorentz factor and viewing angle. Recently, the Event Horizon Telescope (EHT) provided high-resolution imaging of the fine structure of its jet (Kim et al. 2020).

The second source, PKS 2155-304, is a widely studied High-Synchrotron-Peaked BL Lac (HBL) located at $z = 0.116$. It is a bright and variable gamma-ray emitter, first detected at TeV energies in 1996 by the Durham Mark 6 telescope (Chadwick et al. 1999). Since then, it has been regularly monitored by H.E.S.S., revealing log-normal variability behavior and unpredictable extreme flaring events. Some studies have suggested a possible "hard tail" component in its hard X-ray spectrum. Extensive multi-wavelength campaigns have been conducted to constrain its emission mechanisms. Data collected during these campaigns, such as the one in 2008, have been successfully modeled using both leptonic (Synchrotron Self-Compton) and lepto-hadronic scenarios (Aharonian et al. 2009; Cerruti et al. 2012b). Additionally, PKS 2155-304 is being investigated as a potential source of high-energy cosmic rays and neutrinos, although no definitive correlations with neutrino detections (e.g., by ANTARES) have been established to date.

3. Spectral Energy Distribution Modeling of Blazars

To investigate the physical mechanisms responsible for the broadband emission of blazars, a single-zone radiative model is typically adopted. This framework assumes a spherical emission region of radius R, permeated by a magnetic field B, moving with a bulk Lorentz factor Γ within the relativistic jet (Bernardo da Silva et al. 2025; Pereira & Bernardo da Silva 2025). The modeling approaches are generally divided into two main scenarios: purely leptonic and lepto-hadronic.

3.1. Leptonic Modeling

The leptonic model posits that the radiative output is dominated by relativistic electrons and positrons. The Spectral Energy Distribution (SED) exhibits two characteristic peaks: the low-energy peak (radio to X-rays) arises from synchrotron radiation, while the high-energy peak (gamma-rays) is attributed to Inverse Compton (IC) scattering (Spurio 2018).

In the Synchrotron Self-Compton (SSC) scenario, relativistic electrons are injected into the emission region and subsequently upscatter their own synchrotron photons to higher energies. Consistent with the time-dependent framework, we define the electron injection rate, $Q_e(\gamma)$, as a broken power-law distribution:

$$Q_e(\gamma) = Q_{0,e} \begin{cases} \gamma^{-p_1}, & \gamma_{\rm min} \le \gamma \le \gamma_{\rm b} \\ \gamma_b^{p_2-p_1}\gamma^{-p_2}, & \gamma_{\rm b} < \gamma \le \gamma_{\rm max} \end{cases} \quad (1)$$

where $Q_{0,e}$ is the normalization factor (related to the injected luminosity), γ_b is the break Lorentz factor, and p_1, p_2 are the spectral indices (Tramacere et al. 2011; Pereira & Bernardo da Silva 2025). This modeling is computationally performed using the **JetSeT** framework, which utilizes Markov Chain Monte Carlo (MCMC) algorithms to fit the observational data and constrain parameters such as the magnetic field and particle density (Tramacere 2020).

3.2. Lepto-Hadronic Modeling

To explain Very High Energy (VHE) gamma-ray emission and potential neutrino production, lepto-hadronic models include a population of relativistic protons alongside electrons. These protons interact with ambient photon fields (e.g., synchrotron photons) or thermal protons, leading to particle cascades (Mannheim 1993; Rodrigues et al. 2019).

Key hadronic processes include the photomeson production channels:

$$\begin{aligned} &p\gamma \to \Delta^+ \to n\pi^+ \quad (\mathrm{BR} = 2/3) \\ &n \to pe^-\bar{\nu}_e \\ &\pi^+ \to \mu^+\nu_\mu \to e^+\bar{\nu}_\mu\nu_e\nu_\mu \\ &p\gamma \to \Delta^+ \to p\pi^0 \quad (\mathrm{BR} = 1/3) \\ &\pi^0 \to \gamma\gamma \end{aligned} \quad (2)$$

These complex interactions are simulated using the **AM**^{3} (Astrophysical Multi-Messenger Modeling) software, which solves coupled differential equations for the temporal evolution of particle densities, accounting for non-linear effects like electromagnetic cascades (Klinger et al. 2024).

AM^3 solves the system of time-dependent partial differential equations for the differential particle density $n_i(E,t)$ of species i (protons, electrons, photons, etc.):

$$\frac{\partial n_i}{\partial t} = -\frac{\partial}{\partial E}\left(b_i(E)\, n_i\right) - \frac{n_i}{t_{\rm esc}(E)} + Q_i(E,t) \quad (3)$$

where $b_i(E) = -dE/dt$ represents continuous energy losses (such as synchrotron cooling), $t_{\rm esc}$ is the characteristic escape time from the emission region, and $Q_i(E,t)$ is the injection term. The non-linearity and coupling between species arise in the term Q_i, which includes both external injection and the source terms from interactions (Klinger et al. 2024).

For the hadronic component specifically, we assume a power-law injection for the protons. The injection term $Q_p(\gamma)$ in Equation 3 is defined as:

$$Q_p(\gamma) = Q_{0,p}\, \gamma^{-s_p}, \quad \text{for} \quad \gamma_{p,\rm min} \le \gamma \le \gamma_{p,\rm max} \quad (4)$$

where $Q_{0,p}$ is the normalization factor determined by the total proton luminosity. For this work, we adopt a hard spectral index of $s_p = 1.5$ and a minimum proton Lorentz factor of $\gamma_{p,\rm min} = 100$.

4. Methodology

The methodology adopted to investigate the broadband emission and the potential for neutrino emission of the selected blazars combines the collection of multi-wavelength observational data with advanced numerical modeling. The approach is divided into two main stages: the fitting of the Spectral Energy Distribution (SED) via purely leptonic processes and the subsequent simulation of time-dependent lepto-hadronic scenarios.

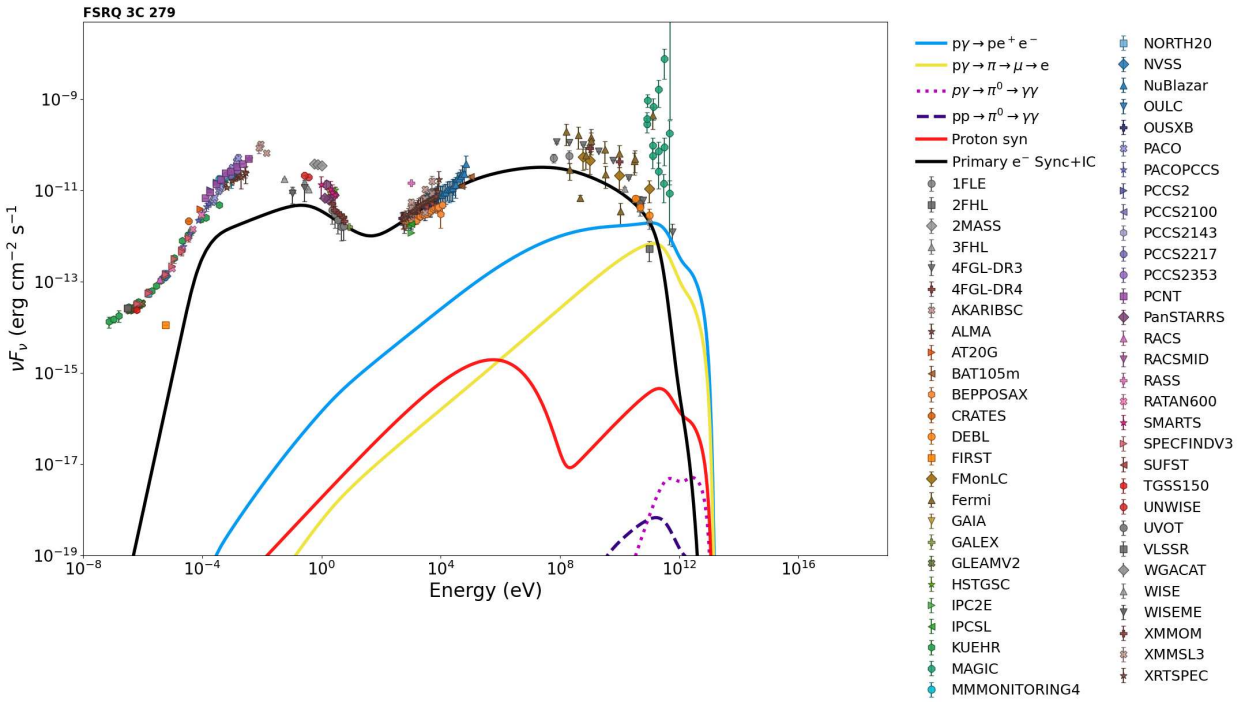

Figure 1. Spectral Energy Distribution (SED) and multi-wavelength data for the FSRQ 3C 279. The markers represent observational data from multiple instruments and catalogs, including Fermi, MAGIC, and others, spanning radio to gamma-ray frequencies. The black solid line represents the primary electron emission (Synchrotron + IC). The colored curves illustrate contributions from various radiation processes modeled using a lepto-hadronic framework: Bethe-Heitler pair production ($p\gamma \to pe^+e^-$, light blue curve) spanning $\sim 10^{-4}$ eV to 10^{13} eV; the charged pion decay cascade ($p\gamma \to \pi^\pm \to \mu^\pm \to e^\pm$, yellow curve) spanning $\sim 10^{-1}$ eV to 10^{13} eV; neutral pion decay from photohadronic interactions ($p\gamma \to \pi^0 \to \gamma\gamma$, pink dotted curve) in the range 10^{10} eV to 10^{13} eV; neutral pion decay from proton-proton collisions ($pp \to \pi^0 \to \gamma\gamma$, purple dashed line) in the range 10^9 eV to 10^{12} eV; and proton synchrotron emission (red solid line) from $\sim 10^{-2}$ eV to 10^{12} eV. Source: Author.

4.1. Multi-wavelength Data

To construct comprehensive SEDs, covering radio to very high energy (VHE) gamma-rays, archival data from various ground-based and space-borne observatories were utilized. The compilation of this data was performed using specialized tools, primarily the **Space Science Data Center (SSDC)**. Managed by the Italian Space Agency (ASI), this infrastructure provides access to historical data and products from high-energy missions. Additionally, we employed **Firmamento**, a web-based platform designed to aggregate and visualize photometric data from various sources, which facilitated the construction of the SEDs required for the modeling process.

4.2. Numerical Modeling

The physical interpretation of the observational data was carried out using two open-source codes, each focused on a specific interaction regime.

4.2.1. Leptonic Modeling with JetSeT

The initial modeling of the electromagnetic emission was conducted using the **JetSeT** software (version 1.3.0). This code, implemented in C and Python, simulates radiative and acceleration processes in relativistic jets. We adopted a single-zone model, where the emission region is approximated by a homogeneous sphere of radius R, permeated by a magnetic field B, and moving with a bulk Lorentz factor Γ. regarding the radiative processes, the model considers Synchrotron emission and Inverse Compton scattering (SSC — Synchrotron Self-Compton), where relativistic electrons upscatter their own synchrotron photons to higher energies. The electron distribution is described by a broken power-law. To determine the best-fit parameters and associated uncertainties, the parameter space was explored using a Bayesian approach via the Markov Chain Monte Carlo (MCMC) algorithm.

4.2.2. Lepto-Hadronic Modeling with AM^3

To investigate the hadronic contribution and possible neutrino emission, the **AM^3** (Astrophysical Multi-Messenger Modeling) software was used. This framework solves systems of coupled differential equations to describe the temporal evolution of the densities of photons, electrons, positrons, protons, neutrons, pions, muons, and neutrinos. The model incorporates photohadronic interactions ($p\gamma$), including Bethe-Heitler pair production ($p\gamma \to pe^+e^-$) and photopion production ($p\gamma \to N\pi$), as well as proton-proton collisions (pp). A key feature of AM^3 is its consistent treatment of non-linear effects, such as electromagnetic cascades initiated by the decay of secondary pions and muons, which redistribute energy to lower frequencies. To ensure the physical viability of the model, the injected proton luminosity is typically constrained by or compared to the Eddington luminosity of the central black hole.

5. Results and Discussion

The modeling of the Spectral Energy Distribution (SED) for the sources 3C 279 and PKS 2155-304 was performed by adopting

Table 1. Parameters for the sources PKS 2155-304 and 3C 279. The proton spectral index was fixed at $s_p = 1.5$ and the minimum proton Lorentz factor at $\gamma_{p,\min} = 100$.

Parameter	PKS 2155-304	3C 279
z	0.12	0.54
B [G]	1.99×10^{-2}	1.00×10^{-2}
R [cm]	1.21×10^{16}	3.34×10^{17}
$N_{0,e}$ [cm^{-3}]	10.46	16.16
$p_{1,e}$	1.59	2.47
$p_{2,e}$	3.63	3.84
$E_{\min,e}$ [eV]	3.69×10^{7}	1.53×10^{8}
$E_{\text{break},e}$ [eV]	4.70×10^{9}	6.64×10^{9}
$E_{\max,e}$ [eV]	1.01×10^{12}	5.41×10^{13}
$E_{\min,p}$ [eV]	9.38×10^{10}	9.38×10^{10}
$E_{\max,p}$ [eV]	1.75×10^{15}	1.00×10^{18}
θ [°]	0.24	3.55
Γ_{bulk}	50.0	12.32
R_H [cm]	1.0×10^{17}	1.0×10^{17}
L_e [erg s^{-1}]	2.61×10^{44}	1.71×10^{46}
L_p [erg s^{-1}]	2.62×10^{44}	1.72×10^{46}

a hybrid approach. Initially, we used the *JetSeT* code to fit the leptonic components (Synchrotron and SSC), represented by the black curves in Figures 1 and 2. Subsequently, we used the *AM*^{3} software to calculate the lepto-hadronic contributions, which are essential for describing the emission at extreme energies.

The physical parameters resulting from the best fit for the sources PKS 2155-304 and 3C 279 are detailed in Table 1. These values were initially obtained through leptonic modeling using *JetSeT* to describe the synchrotron and SSC emission, and served as the basis for particle injection in the lepto-hadronic scenario simulated with *AM*^{3}. We observe that both objects present relatively low magnetic fields ($B \sim 10^{-2}$ G), typical of emission regions located at a significant distance from the central black hole, where the particle energy density tends to dominate over the magnetic energy density.

For the FSRQ 3C 279, the emission region (R) and the total jet luminosity (L_e, L_p) are significantly larger than for the BL Lac PKS 2155-304, consistent with the higher intrinsic luminosity of quasars. On the other hand, PKS 2155-304 required an extremely high bulk Lorentz factor ($\Gamma_{\text{bulk}} = 50$) to fit the high-energy emission, indicating a strong relativistic *beaming* effect. In the proposed lepto-hadronic scenario, we assumed an approximate equipartition condition between the electron and proton luminosities ($L_e \approx L_p$), allowing protons to reach maximum energies ($E_{\max,p}$) of the order of 10^{18} eV for 3C 279, classifying it as a possible accelerator of ultra-high-energy cosmic rays (UHECRs).

5.1. FSRQ 3C 279

Figure 1 presents the fit for the FSRQ 3C 279. It is observed that the purely leptonic model (solid black line) adequately reproduces the emission from radio frequencies up to the X-ray band, corresponding to the synchrotron peak and the low-energy part of the Compton peak. However, to explain the emission in the high-energy (HE) and very-high-energy (VHE) gamma-ray bands, the lepto-hadronic scenario proves to be fundamental.

The colored curves in Figure 1 illustrate the importance of proton-photon interactions ($p\gamma$). Pair production via the Bethe-Heitler process ($p\gamma \rightarrow pe^+e^-$, light blue line) and the electromagnetic cascade resulting from pion decay ($p\gamma \rightarrow \pi \rightarrow \mu \rightarrow e^{\pm}$, yellow line) provide a significant contribution above 100 MeV, filling the spectrum where the standard SSC model tends to decay abruptly. Proton synchrotron emission (red line) appears as a sub-dominant component but contributes to the overall structure of the spectrum at intermediate energies.

5.2. PKS 2155-304

For the high-frequency peaked BL Lac (HBL) object PKS 2155-304, presented in Figure 2, the synchrotron peak is located at higher frequencies compared to 3C 279, extending into the hard X-ray band. The leptonic fit describes the first part of the spectrum well.

In the VHE (TeV) region, modeling with *AM*^{3} reveals that the emission can be consistently explained by the superposition of primary electron emission with secondary hadronic components. The contribution of the Bethe-Heitler process (light blue line) and photopion decay products (yellow line) is crucial for modeling the high-energy tail observed by Cherenkov telescopes, such as H.E.S.S. Furthermore, the presence of these hadronic interactions suggests that the source is an efficient cosmic ray accelerator, with proton luminosities that may reach values close to the Eddington luminosity during periods of high activity.

6. Conclusion

In this work, we investigated the multi-wavelength emission of the blazars 3C 279 and PKS 2155-304 through detailed numerical modeling that combines leptonic and lepto-hadronic processes. Our results indicate that:

1. The single-zone leptonic model (Synchrotron + SSC) is sufficient to explain the emission from radio up to X-rays, providing robust constraints on the magnetic field and electron density in the emission region.
2. The inclusion of hadronic components, simulated via *AM*^{3}, is essential to reproduce the complexity of the gamma-ray spectrum (GeV-TeV), especially to explain the spectral hardening observed at high energies.
3. The Bethe-Heitler and photopion production processes play a central role in the generation of secondary electrons and positrons, which, in turn, contribute via Compton scattering and synchrotron emission to the observed SED.

These results reinforce the hypothesis that blazars are possible sources of ultra-high-energy cosmic rays and promising candidates for the future detection of astrophysical neutrinos correlated with VHE photon emission. Future observations with next-generation instruments, such as the CTAO (*Cherenkov Telescope Array Observatory*), will be fundamental to unequivocally distinguish between the proposed purely leptonic and lepto-hadronic scenarios.

Acknowledgements. S.V.B. da Silva gratefully acknowledges financial support from CAPES and PPGCosmo. L.A.S. Pereira gratefully acknowledges financial support from FAPESP under grant numbers 2021/01089-1, 2024/02267-9, and 2024/14769-9, and from CNPq under grant numbers 403337/2024-0, 153839/2024-4, and 200164/2025-2.

References

Abdalla, H., Adam, R., Aharonian, F., et al. 2019, A&A, 639, A37
Aharonian, F., et al. 2009, ApJL, 696, L150
Bernardo da Silva, S. V., Stuani Pereira, L. A., & Dos Anjos, R. C. 2025, Universe, 11, 177
Bharathan, A. M., Stalin, C. S., Sahayanathan, S., & Mathew, B. 2025, arXiv:2509.16976
Bovy, J. 2015, ApJS, 216, 29
Cerruti, M., Zech, A., Boisson, C., & Inoue, S. 2012a, AIP Conf. Proc., 1505, 635

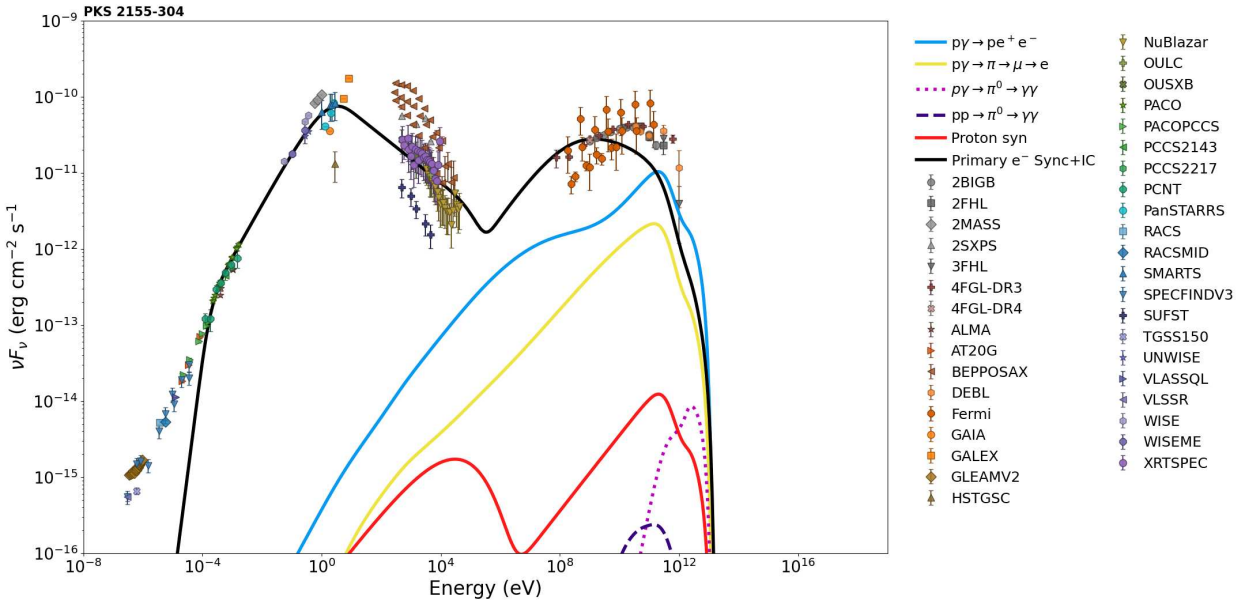

Figure 2. Spectral Energy Distribution (SED) and multi-wavelength data for PKS 2155-304. The markers represent observational data from multiple instruments and catalogs, including Fermi, H.E.S.S., and others, spanning radio to gamma-ray frequencies. The black solid line represents the primary electron emission (Synchrotron + IC). The colored curves illustrate contributions from various radiation processes modeled using a lepto-hadronic framework: Bethe-Heitler pair production ($p\gamma \to pe^+e^-$, light blue curve) spanning $\sim 10^0$ eV to 10^{13} eV; the charged pion decay cascade ($p\gamma \to \pi^\pm \to \mu^\pm \to e^\pm$, yellow curve) spanning $\sim 10^2$ eV to 10^{13} eV; neutral pion decay from photohadronic interactions ($p\gamma \to \pi^0 \to \gamma\gamma$, pink dotted curve) in the range 10^{11} eV to 10^{13} eV; neutral pion decay from proton-proton collisions ($pp \to \pi^0 \to \gamma\gamma$, purple dashed line) in the range 10^{10} eV to 10^{12} eV; and proton synchrotron emission (red solid line) from $\sim 10^1$ eV to 10^{12} eV. Source: Author.

Cerruti, M., et al. 2012b, AIP Conf. Proc., 1505, 635
Chadwick, P. M., et al. 1999, ApJ, 513, 161
Errando, M., et al. 2008, AIP Conf. Proc., 1085, 423
Harutyunyan, G., Sahakyan, N., Bégué, D., & Khachatryan, M. 2025, arXiv:2509.11827
Hartman, R. C., et al. 1992, ApJL, 385, L1
Kim, J., et al. 2020, A&A, 640, A69
Klinger, M., et al. 2024, ApJS, 275, 4
Krishna Mohana, A., Gupta, A. C., Fan, J. H., et al. 2025, arXiv:2507.03913
Lucchini, M., Markoff, S., Crumley, P., et al. 2018, MNRAS, 482, 4798
Lynds, C. R., Stockton, A. N., & Livingston, W. C. 1965, ApJ, 142, 1667
Mannheim, K. 1993, A&A, 269, 67
Pereira, L. A. S. & Bernardo da Silva, S. V. 2025, submetido
Petropoulou, M. 2014, A&A, 571, A87
Petropoulou, M., et al. 2015, MNRAS, 448, 2412
Rodrigues, X., et al. 2019, ApJL, 874, L29
Spurio, M. 2018, Probes of Multimessenger Astrophysics, Springer
Tramacere, A. 2020, ASCL, ascl:2009.001
Tramacere, A., Massaro, E., & Taylor, A. M. 2011, ApJ, 739, 66
Weidinger, M. & Spanier, F. 2010, IJMPD, 19, 887